Design of Error Tolerant Coupling Mechanisms for Metamorphic Robots

Amit Pamecha Yas Kohaya Gregory Chirikjian
Department of Mechanical Engineering
Johns Hopkins University
Baltimore, MD 21218

Abstract

Metamorphic robots consist of a collection of mechatronic modules which can connect, disconnect and move around each other. An important aspect of the hardware implementation of such robots is the coupling mechanism which helps to connect and disconnect the modules. The design of the coupling has to take into account the misalignment of mating links due to the finite link thickness and use as little power as possible while carrying load at the same time. In this paper a mechanically error tolerant coupling mechanism for planar metamorphic robot is described which satisfies the above constraints. Hardware implementation of the above design is demonstrated for the case of hexagonal modules.

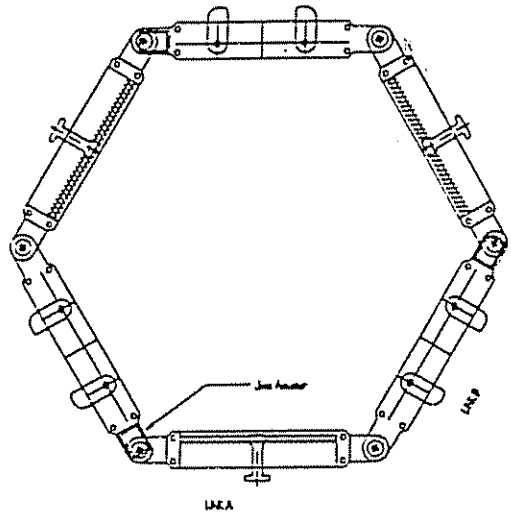

Figure 1: The mechanical structure of a module.

1 Introduction

A *metamorphic* robotic system [Ch94] is a collection of independently controlled, kinematically sufficient, mechatronic modules, each of which has the ability to connect, disconnect, and climb over adjacent modules. A metamorphic system has the ability to dynamically reconfigure by the locomotion of modules over their neighbors. Thus they can be viewed as a collection of connected modular robots which act together to perform the given task.

Some important characteristics of *metamorphic* systems are

1. All modules are identical in physical structure and are computationally self-contained.

2. The modules possess a certain degree of symmetry so as to fill planar or spatial regions with minimal gaps.

3. The modules are kinematically sufficient.

4. Modules possess the ability to connect and disconnect with adjacent modules.

One of the designs which satisfies all the above properties in the planar case involves the use of hexagonal modules. Each module, as shown in Figure 1, consists of six links of equal length forming a six bar linkage. Because of the hexagonal shape, the modules completely fill the plane without any gaps. The centers of the modules form a regular lattice and thus each module can be treated as part of a lattice structure. As can be seen from the figure, each module possesses three degrees of freedom which are controlled by placing actuators at alternate joints. This enables each module to move around another while remaining connected at all times during this motion (see Figure 2).

The modules are provided with electromechanical connectors or coupling mechanism actuated by D.C. motors. Each module carries male and female connectors on alternate links. Because of the symmetry of the module, male connectors always meet female connectors and vice-versa [Ch94]. Each module must also contain a microprocessor which controls the link actuators and the connector motors making the module computationally self-contained.

One of the most important aspects of the above design is the coupling or the connector mechanism. The connector not only has to adhere to the adjacent module but also has to allow sliding motion of the links because of finite link thickness (discussed in detail later). In addition it should be a passive or a quasi-passive mechanism so as to use minimum power i.e, once it has coupled or uncoupled the modules, it should require no power to maintain the connection.

This paper deals with issues in the design of *error-tolerant* coupling mechanisms for metamorphic robots, i.e the coupling mechanism can take into account wide variations in connector position on the mating link. Section 2 contains a brief literature review. In section 3 we describe the locomotion of hexagonal modules. Section 4 describes some alternatives in the design of couplings for such modules. Section 5 discusses the design and implementation of an error tolerant connector mechanism satisfying the above conditions. Section 6 presents results and conclusions.

2 Literature Review

The idea of a metamorphic robotic systems differs from related concepts presented in the literature. Three types of modular reconfigurable robotics systems have been proposed in the literature: (1) robots in which modules are reconfigured using external intervention, e.g., [BeZL89, CoLDB92, Sci85, W86]; (2) cellular robotic systems in which a heterogeneous collection of independent specialized modules are coordinated, e.g., [Be88, BeW91, FuN88, FuK90]; (3) swarm intelligence in which there are generally no physical connections between modules, e.g., [HaB91]. The concept of a metamorphic system is separate from all of the above because modules are homogeneous in form and function, contact between modules must always occur, and self-reconfiguration is possible. The concept of metamorphic systems was introduced in [Ch94], and a closely related problem is examined in [MKK94].

In the present work, where the design of a mechanically error tolerant coupling mechanism is examined, another body of literature is important. Namely, work that deals with the mechanics of pushing and friction and work that uses geometric and physical constraints to guarantee desired performance with minimal numbers of crude sensors, e.g., [AkM92,CaG94,ErM88,Ma93,PeS89,PeBG93, RaG94]. By using this 'minimalist' philosophy, we have developed a coupling device for metamorphic robots that requires no sensors and has a geometry that allows for significant errors. This is important because a metamorphic robotic system may frequently need to reconfigure, and so the connection between modules must be reliable.

3 Locomotion of Modules

The reconfiguration of metamorphic robots takes place by the locomotion of modules around each other while remaining connected to each other at all times. This can also be described as the 'rolling' of one module over others. Figure 2 illustrates the locomotion procedure. Observe that the module which is moving remains connected to the other module during the entire process. For clarity, let's define the module which is moving at a given time to be *mobile* and the module over which it moves to be *fixed*. The motion of the *mobile* module is achieved by controlling the three degrees of freedom of the module by three actuators on alternate joints. For a detailed description of the kinematics of the mechanism and how joint angles are altered see [Ch94].

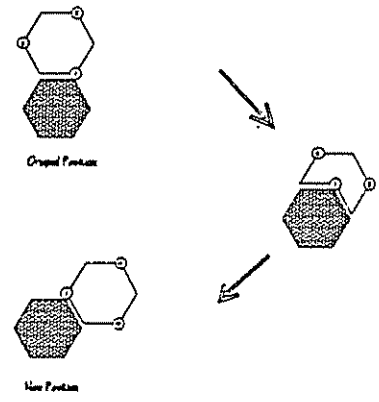

Figure 2: The locomotion of one module over another. One of the links of the *mobile* module always remains connected to the *fixed* module.

As described before, adjacent links of the modules carry male and female connectors, or in other words, they are of opposite 'polarity'. Because of the symme-

try of the modules, the locomotion always results in links with opposite polarity or male/female connectors meeting with each other. In addition this symmetry is maintained over the entire structure, i.e. the adjacent links on the boundry of the collection of all modules are of different polarity. See Figure 3.

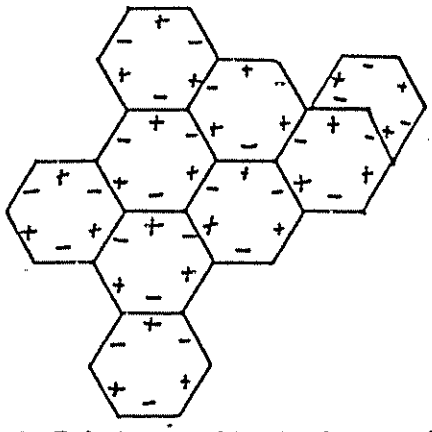

Figure 3: Polarity matching in the reconfiguration of metamorphic robot.

Any implementation of the locomotion process described above in practice has problems because of the finite thickness of the links.Due to the finite thickness, the axes of rotation of the joints of two mating links are not coincident. As a result, when a module moves over the other, the links in the new position are not aligned. For an illustration of this see Figure 4. The displacement (d) between the two links is a function of the width (w) of the links and is given as

$$d = w \tan\theta$$

where θ is 30°. This can be derived very simply by observing the module geometry in figure 4. If this displacement or misalignment is not eliminated, the next motion of the module in the same direction cannot take place. Another problem due to this misalignment and due to the possibility of motion in both clockwise and counterclockwise directions is that the connectors on the two opposite links do not meet at an exact point on the links, i.e. the connectors themselves get displaced with respect to each other.

An alternative strategy for motion is one in which the *fixed* and the *mobile* modules move together so that the old connection and the new one are parallel to the mating links, i.e. each of the two mating links moves by 60° towards each other instead of the link of the *mobile* module moving by 120°. This ensures proper alignment but requires a coordinated simultaneous movement of other modules in the structure.

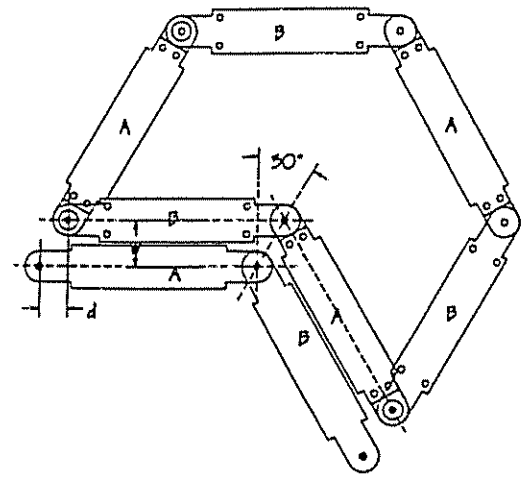

Figure 4: Displacement between the links due to finite link thickness

The above argument indicates that the locomotion procedure of modules warrants a mechanism that somehow removes the displacement between the links. Also, since the connectors do not meet at the same position relative to the links, an error tolerant connector mechanism is required. The next section discusses some of the alternatives which overcome the above problems.

4 Alternatives in Connector Design

As described in the previous section, the locomotion of modules necessitates the use of a design which aligns the mating links and an error tolerant connector on the two mating links of the modules. A number of possible designs can satisfy the above requirements.

One alternative is to make the links extensible, i.e. the links can contract or expand relative to their normal length. In this case the mating link on the *mobile* module extends (Figure 5, step 1) aligning itself to the link of the *fixed* module (Figure 5, step 2), locks in, releases the old connection and contracts to regain the normal shape (Figure 5, step 3). The obvious problem with this method is that it needs an actuator for each link to extend or contract in addition to the actuators required for the motion of the joints and for locking unlocking of connectors.

Another approach which tries to solve the two problems is one in which the connector is a spring loaded

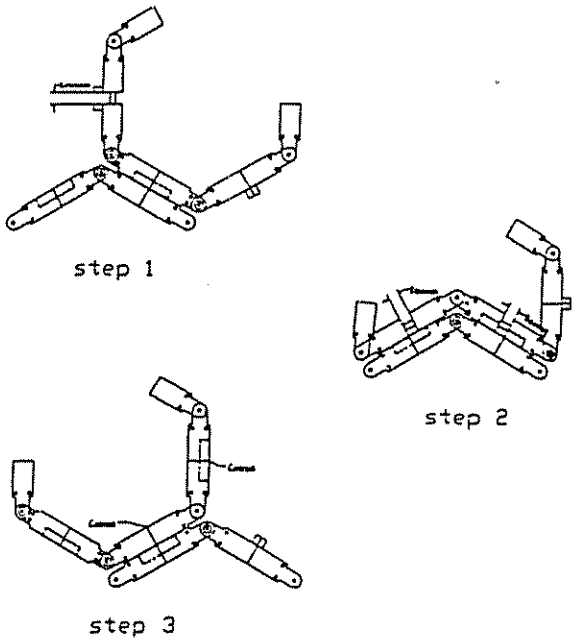

Figure 5: Motion involving link extension and contraction.

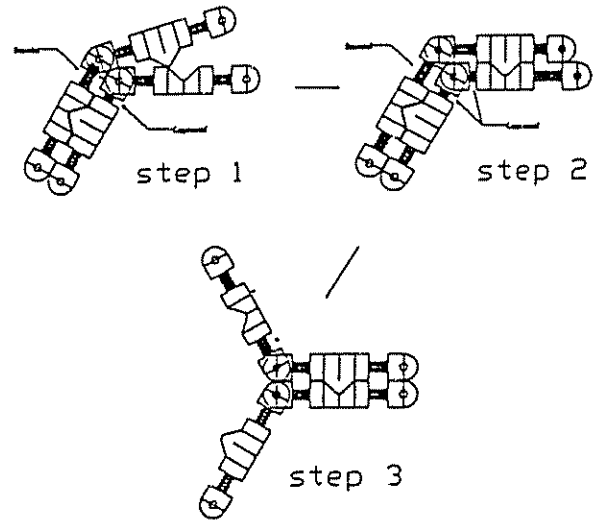

Figure 6: The spring loaded connector shown for two links from each module.

mechanism which aligns the two links together. For an illustration of this see Figure 6. The connector on the link of the *mobile* module slides into a wedge shaped connector on the opposing link by compressing the spring. The relative compression and extension of the springs on the links is given by the minimization of the strain energy function associated with the springs. When the old connection gets released the spring aligns the entire module to normal position. The problem with this method is that for moving the entire module once the old connection gets released, a stiff spring is required. But this necessiates the use of high torque motors for joint motions in order to compress the spring in the first place. The larger actuators in turn increase the weight of the system, which then requires stiffer springs. As a result this design is difficult to implement and increases the power requirement.

Yet another option is to use electromagenetic connectors which serve the dual purpose of aligning the two mating links and connecting the two modules. One design employing such a method is shown in Figure 7. Each link has an electromagnet as a connector. When the old connection is released (by repulsing the electromagnets forming the connection), the electromagnets align the links completely due to magnetic force. The rigid connection between the modules is provided by the magnetic force between the two connectors. A similar scheme has been used by [MKK94] in the development of self-assembling machines or 'fracta'. The problem with this approach is that connection between different modules are active instead of passive. This means that a large amount of power for the electromagnets is required at all times to keep the modules connected.

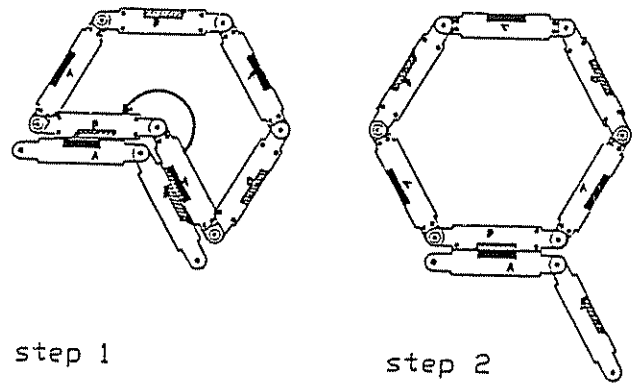

Figure 7: Module motion using electromagnetic coupling.

The next section describes the design of a error tolerant connector which tries to overcome the limitations of the above designs while providing proper alignment and a passive connection between the modules.

5 Error Tolerant Coupling Mechanism

This section describes a coupling mechanism for the mating links of two metamorphic robot modules. The mechanism takes into account the finite link thickness and helps in carrying out the motion as described in section 3.

The coupling mechanism consists of two different types of connectors, referred to as *male* and *female*. Let's define the link carrying the *male* connector as link A and the one carrying the *female* connector as link B. See Figures 8 and 9.

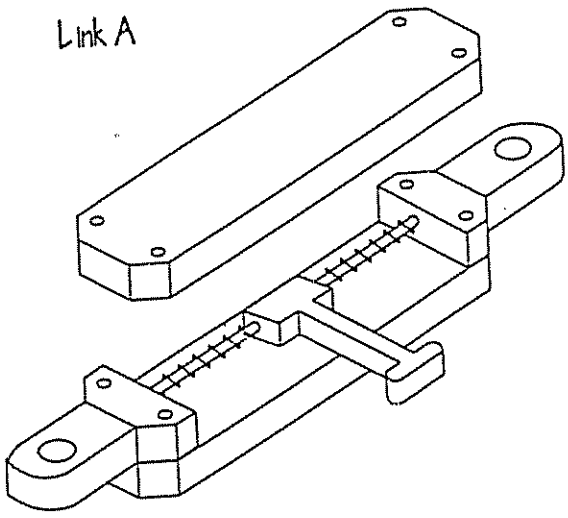

Figure 8: Semi-exploded view of link A showing the spring loaded protrusion.

Link A consists of two parallel plates with space in between. The space carries a T-shaped protrusion mounted on a sliding mechanism. The protrusion is held in place by two springs, one on each side (see Figure 8). As a result, when force is applied to the protrusion, it can slide sideways by compressing the springs.

Link B also consists of two parallel plates with space in between. The space carries two cams, able to rotate 120° about their axes. The cam dimensions are such that when they move in, they completely lock the protrusion on the corresponding link of the other module. The locking of the protrusion by the cams prevents any lateral movement while the T-shaped structure of the protrusion stops any longitudinal movement. The cams are operated in unison by a single actuator (a small DC motor in our case) which is connected to the

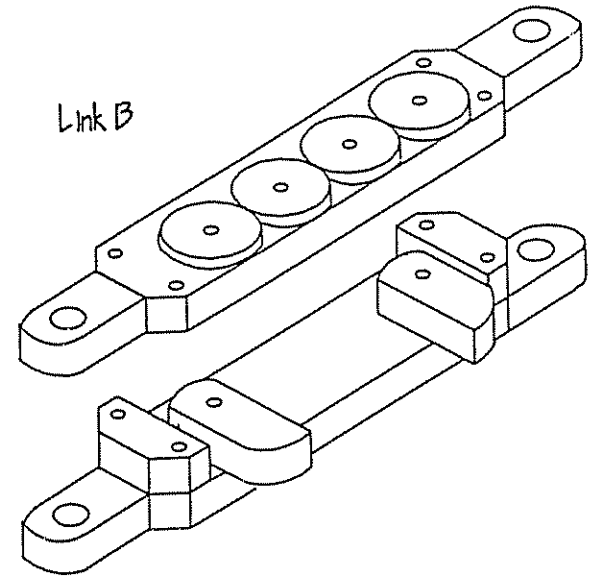

Figure 9: Semi-exploded view of link B showing the double cam mechanism. Shown here without the actuator

cams by a set of 4 gears as shown in Figure 9. As a result the cams open and close simultaneously.

The motion sequence utilizing this mechanism is shown in Figure 10, steps 1 to 4. Step 1 shows the original position of the two adjacent modules, one of which is about to move around the other. In step 2 link A1 of the *mobile* module moves towards link B2 without displacing link B1. In step 3 this motion is continued, but as link A1 moves into B2, it slides the connector on link A2 by compressing one of the springs. As a result, link B1 gets displaced from its original position and shifts sideways. The cams on B2 now close in, aligning link A1 parallel to B2. This results in the connector on A1 getting displaced from it's mean position and one of the springs getting compressed. In step 4 the cams on link B1 open up, releasing the connector on A2. B1 then rotates by 120° and the structure attains the configuration shown in the figure corresponding to step 4. The compressed spring on A1 now aligns link A1 and B2 completely. This completes one move of the module.

As can be seen, only one actuator is needed for each coupling mechanism i.e. one actuator for every two links of the module. The links are aligned exactly by the use of springs on alternate links. A large space is available between the cams(in their open position), as a result the protrusion or the connector on the opposing link can mate from both directions and need not mate at an exact position, i.e. the coupling mechanism

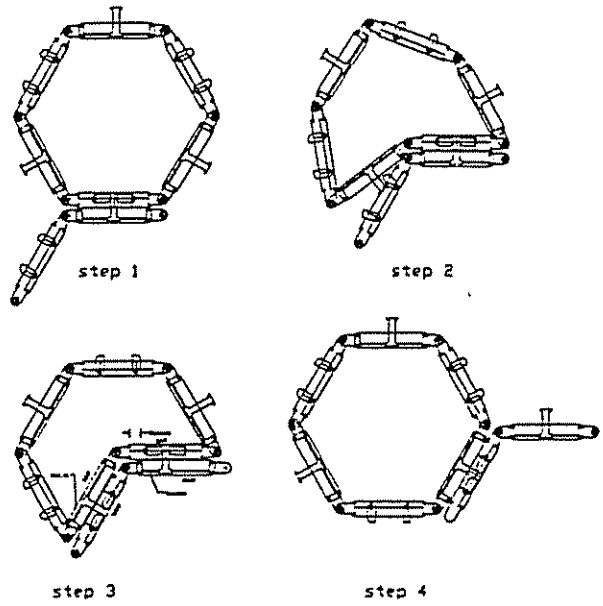

Figure 10: Motion sequence demonstrating action of the error tolerant coupling mechanism.

is *error tolerant*. Another advantage of the above design is that the locking mechanism is passive in the stationary state and so uses very little power.

A working prototype using the above design is shown in Figure 11. For a video of the locomotion process involving error tolerant connectors, see [PCh95]. Presently only two links on each module of the prototype carry the coupling mechanism in order to illustrate the concept. The figures show the different steps in the locomotion process.

6 Conclusion

In this paper we described the design and implementation of an error tolerant coupling mechanism for a planar hexagonal metamorphic robot. The locomotion process for metamorphic robots and alternatives in connector design were discussed. The implemented design overcame the limitations imposed by finite link thickness and had the benefit of being error tolerant. In addition it uses a minimal number of actuators and no power to keep the robot connected in the stationary state.

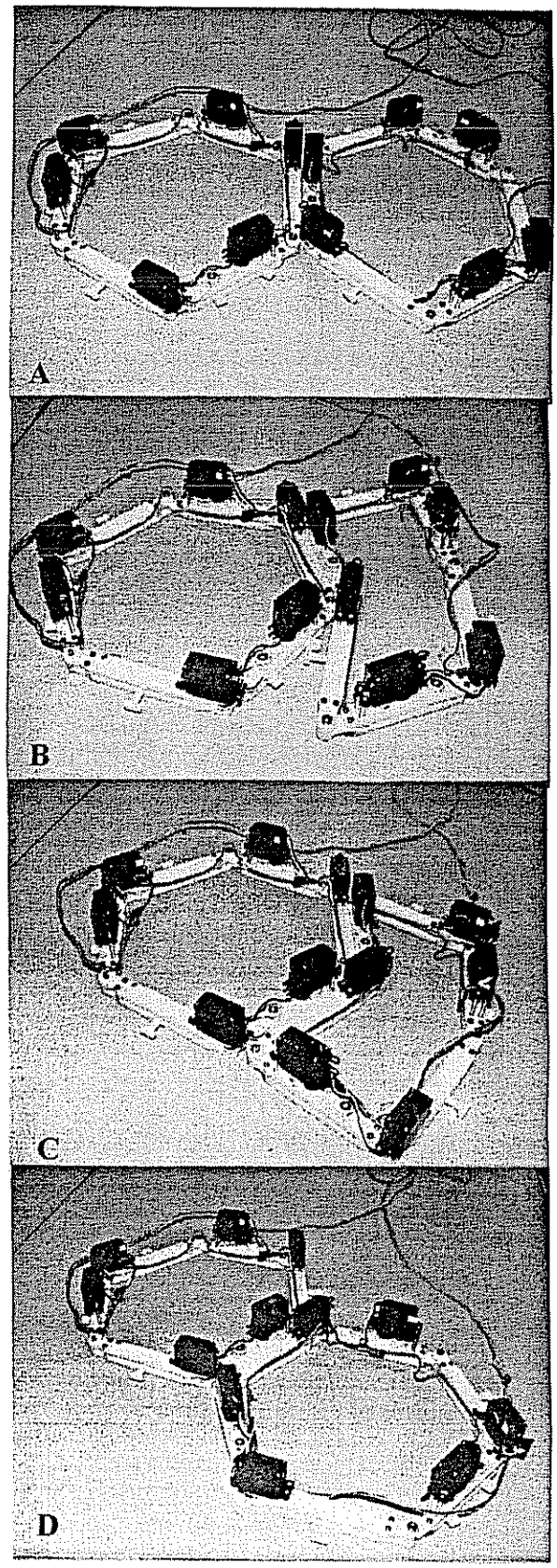

Figure 11: Illustration of the motion sequence with hardware.

7 References

[AkM92] Akella, S., Mason, M.T., "Posing polygonal objects in the plane by pushing," Proc. IEEE 1992 International Conference on Robotics and Automation, pages: 2255-2262.

[BeZL89] Benhabib, B., Zak, G., Lipton, M.G., "A Generalized Kinematic Modeling Method for Modular Robots," *Journal of Robotic Systems*, vol. 6, No. 5, 1989, pp. 545-571.

[Be88] Beni, G., "Concept of Cellular Robotic Systems," *IEEE Int. Symposium on Intelligent Control*, Arlington, VA, August 24-26, 1988

[BeW91] Beni, G., Wang, J., "Theoretical Problems for the Realization of Distributed Robotic Systems," *1991 IEEE Conf. on Robotics and Automation*, 1991, pp. 1914-1920.

[CaG94] Canny, J., Goldberg, K., " A RISC approach to robotics," IEEE Robotics and Automation Magazine, pages: 26-28, March 1994.

[Ch94] Chirikjian, G.S., "Kinematics of a Metamorphic Robotic System," *Proceedings of the 1994 IEEE Int. Conf. on Robotics and Automation*, San Diego, CA, May 1994, pp.449-455.

[PCh95] Pamecha, A., Chirikjian, G.S., "A Metamorphic Robotic System : Simulation and Connector Mechanism Demonstration," (Video Submission, *1995 IEEE International Conference on Robotics and Automation.*)

[CoLDB92] Cohen, R., Lipton, M.G., Dai, M.Q., Benhabib, B., "Conceptual Design of a Modular Robot," *Journal of Mechanical Design*, March 1992, pp. 117-125.

[ErM88] Erdmann, M.A., Mason, M.T., "An exploration of sensorless manipulation," IEEE Journal of Robotics and Automation, Vol.4, No.4, August 1988.

[FuN88] Fukuda, T., Nakagawa, S., "Dynamically Reconfigurable Robotic Systems," *Proc. 1988 IEEE Conf. on Robotics and Automation*, pp. 1581-1586

[FuK90] Fukuda, T., Kawauchi, Y., "Cellular Robotic System (CEBOT) as One of the Realization of Self-organizing Intelligent Universal Manipulator," *Proc. 1990 IEEE Conf. on Robotics and Automation*, pp. 662-667.

[HaB91] Hackwood, S., Beni, G., "Self-organizing Sensors by Deterministic Annealing," *IROS'91*, Osaka, Japan, pp. 1177-1183.

[Ma93] Mason, M.T., "Kicking the sensing habit," AI Magazine, pages 58-59, Spring 193.

[MKK94] Murata, S., Kurokawa, H., Kokaji, S., "Self-Assembling Machine," *Proceedings of the 1994 IEEE Int. Conf. on Robotics and Automation*, San Diego, CA, May 1994, pp.441-448.

[PeS89] Peshkin, M.A., Sanderson, A.C., "Planning robot manipulation strategies for workpieces that slide," IEEE Journal of Robotics and Automation, Vol.4, No.5, Oct-ber 1988.

[PeBG93] Peshkin, M.A., Brokowski, M., Goldberg,K.,"Curved fences for part alignment," Proc. IEEE 1993 International Conference on Robotics and Automation, pages: 467-473.

[RaG94] Rao, A.S., Goldberg, K.Y., "Shape from diameter: Recognizing polygonal parts with a parallel-jaw gripper," International Journal of Robotics Research, Vol.13, No.1, February 1994.

[Sci85] Sciaky, M., "Modular Robots Implementation," *Handbook of Industrial Robotics*, S. Nof, ed., John Wiley and Sons, New York, 1985, pp. 759-774.

[W86] Wurst, K.H., "The Conception and Construction of a Modular Robot System," *Proceedings of the 16th International Symposium on Industrial Robotics*, pp. 37-44, ISIR, 1986

Generation of Binary Manipulator Workspaces and Work Envelopes

Imme Ebert-Uphoff* Gregory S. Chirikjian†
Department of Mechanical Engineering
Johns Hopkins University
Baltimore, MD 21218

Abstract

A binary manipulator is a discrete manipulator whose actuators have only two states. We present an efficient algorithm for the approximation of workspaces and work envelopes for binary manipulators of highly actuated structure. The approximation describes not only the shape of the workspace, but also its local point density, i.e. the distribution of the number of points per unit area/volume. This characteristic of manipulator workspaces and work envelopes is of great practical importance for binary manipulators for a variety of problems, e.g., inverse kinematics and obstacle avoidance.

The method extends naturally to the continuous range-of-motion case for any manipulator that can be approximated as a binary manipulator with a sufficiently large number of bits. This is particularly useful for manipulators with low resolution, since the point density provides a measure for the local positional accuracy of the end-effector.

1 Introduction

The traditional assumption in robotics is that mechanisms are actuated with continuous-range-of-motion actuators such as d.c. motors. However, there are many applications of mechanisms and robotic manipulators that require only discrete motion. For these tasks, continuous-range-of-motion machines are overkill.

A binary actuator is one type of discrete actuator which has only two stable states (denoted '0' and '1'). As a result, binary manipulators have a finite number of states. Major benefits of binary actuation are that extensive feedback control is not required, task repeatability can be very high, and two-state actuators are generally very inexpensive (e.g., solenoids, pneumatic cylinders, etc.), thus resulting in low cost robotic mechanisms.

In principle, an analogy can be made between continuous vs. binary manipulators and analog vs. digital circuits. In the history of electronics and computing, digital devices replaced many of their analog counterparts because of higher reliability and lower cost - exactly the same reasons for developing a binary paradigm for robotics [1].

The goal of this paper is to develop an efficient algorithm for the approximation of binary manipulator workspaces and work envelopes for highly actuated structures. The *workspace*, $W \subset \mathbb{R}^N$, is the set of all positions reachable by the end-effector. A *work envelope* is the boundary of the smallest simply connected subset of $\mathbb{R}^N$ which contains the whole manipulator structure undergoing all configurations of the manipulator.

The importance of manipulator workspace properties for design considerations is well known, e.g., [2, 3], as is the importance of manipulator work envelopes, especially in the context of obstacle avoidance.

In this paper, we explicitly consider binary manipulator workspaces and work envelopes. The methodology can be adjusted to analyze general discrete manipulators, and extends to the continuous range-of-motion manipulators if they can be approximated as binary manipulators with a large number of bits. Note that the approximation describes not only the shape of the workspace, but also its local point density (precise definition to follow). For manipulators with low resolution this is useful, since the point density provides a measure for the local positional accuracy of the end-effector, in this context see [4, 5]

The number of configurations that a binary manipulator can attain is of the form 2^n where n is the number of binary actuators. In order to reach a large number of points n tends to be large for binary manipulators. It is easy to see that for n large enough (e.g., $n \approx 40$) the explicit computation and storage of all workspace points becomes impractical. Therefore an algorithm to determine binary manipulator workspaces and work envelopes for large n becomes necessary.

A schematic of a highly actuated prototype is shown in Figure 1 for two of its almost thirty three thousand (2^{15}) end-effector positions. This particular design is a variable geometry truss manipulator. As currently configured, this manipulator consists of 15 identical prismatic actuators, each with two stable states: completely retracted, 0, or completely extended, 1. The actuator lengths here are respectively 3/20 and 5/20. The platform widths are each 1/5. For this protoype it is still possible to calculate all points of the workspace explicitely by enumerating all configurations (Figure 2). This workspace will be used

*Graduate Student
†Assistant Professor, Presidential Faculty Fellow

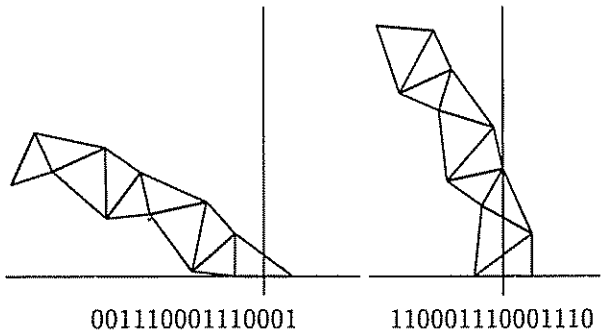

Figure 1: Sample configurations for a manipulator with 5 cascaded platforms

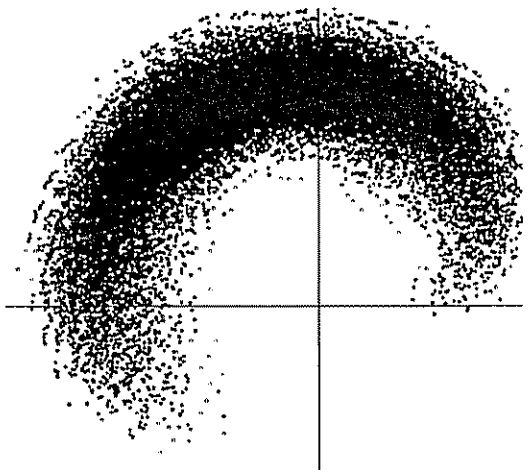

Figure 2: Workspace for a manipulator with 5 cascaded platforms

for a comparison with the output of the algorithm presented in this paper.

The remainder of this paper is organized as follows: Section 2 presents the necessary background and definitions needed to formalize our approach. Section 3 presents the *workspace mapping algorithm* (our approximation algorithm for binary manipulator workspaces). Section 4 presents numerical examples and applies the algorithm to the development of work envelopes. Section 5 is the conclusion.

2 Background Concepts and Definitions

The goal of this section is to provide background needed to develop an efficient algorithm for the approximation of binary manipulator workspaces and work envelopes.

Intuitively, the approach presented here is to break up the workspace into pixels, and calculate how many end-effector positions in each one are reached. This is done efficiently with an algorithm that superposes the contributions of each section of the manipulator by performing recursive homogeneous transformations starting at the end-effector and terminating at the base. In a sense, the whole workspace is generated by repeatedly performing a discrete convolution product of the workspaces associated with individual segments of the manipulator. The computation of the work envelope is also a superposition of the workspaces of subsections of the manipulator, but these computations start at the base and work upwards.

The computations required by our algorithm to generate the workspace for a manipulator composed of m concatenated modules of a given module design, are of order $\mathcal{O}(m)$, where the slope depends on the design of the module. The work envelope is generated using m runs of the workspace algorithm, and therefore requires $\mathcal{O}(m^2)$ computations.

The quantity calculated by the algorithm is called the *point density* of the workspace and will be represented by something called a *density array* (precise definitions to follow). The latter is a computer representation of the number of end-effector points for each pixel of the workspace.

The following subsections present the necessary background and definitions to formalize our approach. This background is necessary because the workspace description for a binary manipulator is different from that of standard continuous range-of-motion manipulators. Subsection 2.1 presents notation and definitions. Subsection 2.2 discusses the storage of information needed for the mapping algorithm.

2.1 Concepts for Discrete Workspaces

The workspace of a continuous range-of-motion manipulator is often described by its boundary, all points in the interior of which can be reached. For a binary manipulator the situation is quite different since only a finite number of points can be reached. Therefore not only the boundary of the workspace is important, but also the distribution of the points inside this boundary.

From now on we assume that the manipulator workspace W (a subset of $\mathbb{R}^N$) is divided into blocks (pixels) of equal size. The distribution of the points is described as follows: The *point density* ρ assigns each block of $W \subset \mathbb{R}^N$ the number of points within the block that are reachable by the binary manipulator, normalized by the volume of the block:

$$\rho(\text{block}) = \frac{\#\text{ reachable points in block}}{\text{unit volume/area}}$$

The point density serves as a probabilistic measure of the positional accuracy of the end-effector in a certain area of the workspace. The higher the density in the neighborhood of a point, the more accurately we expect to be able to reach the point.

The *density array* is an N-dimensional array of integers ($D(i,j)$ for $N = 2$ or $D(i,j,k)$ for $N = 3$) in which each element corresponds to one block of the workspace and contains the number of reachable points in this block. The density array provides a discretized version of the

workspace from which point density is trivially calculated (multiplication with a constant). Furthermore, the shape of a workspace is approximated by all blocks for which the corresponding entry in the density array is not zero.

The following definition specifies the type of manipulator for which our algorithm is used. A *macroscopically-serial manipulator* is a manipulator that is serial on a large scale, i.e. it can be represented by a serial collection of modules where each module is mounted on top of the previous one. Modules are numbered 1 to B, from the base to the end of the manipulator. Closed loops may exist in each module, but macroscopic loops are not permitted. Note: any module partitions a macroscopically-serial manipulator into distinct segments.

The i^{th} *(upper) intermediate workspace*, W_i^I, of a macroscopically serial manipulator composed of B modules is the workspace of the manipulator segment from module $i+1$ to the end-effector. The i^{th} *(lower) partial workspace*, W_i^P, of the same manipulator is the workspace of the segment from the base to module i. To visualize this, imagine that the manipulator arm is cut between module i and module $i+1$. The upper part (the most distal $B-i$ modules) are considered as a manipulator on its own, with its base in the separating plane. The workspace generated by this manipulator segment is the ith intermediate workspace of the whole structure. The lower part (the first i modules) determine the i^{th} partial workspace.

The *workspace mapping algorithm* is based on the sequential calculation of the intermediate workspaces, starting at the end-effector and ending at the base. The fact that these workspaces are the intermediate results of the algorithm is responsible for the naming. The partial workspaces are only used for the generation of work envelopes.

Each module has a frame attached to its top. The frames are numbered such that frame i is on top of module i, and frame 0 is the frame at the manipulator base. The number of independent binary actuators in module i is denoted J_i. Therefore there exist 2^{J_i} different combinations of binary actuator states (and corresponding configurations) for the i^{th} module. Each module i with J_i binary joint angles, for $i = 1, \ldots, B$ will be represented by the *configuration set*:

$$C_i = \{(\mathbf{R}_1, \mathbf{b}_1), (\mathbf{R}_2, \mathbf{b}_2), \ldots, (\mathbf{R}_{2^{J_i}}, \mathbf{b}_{2^{J_i}})\},$$

where $\mathbf{R}_j \in \mathbf{SO(N)}$ are rotation matrices and $\mathbf{b}_j \in I\!R^N$ are translation vectors for $j = 1, \ldots, 2^{J_i}$. These pairs describe all possible relative orientations and positions of frame i with respect to frame $i-1$.

2.2 Efficient Representation of Workspaces

Our algortihm is based on determining intermediate workspaces in sequence. Therefore a conceptual tool is needed to efficiently store intermediate workspaces for future use. Efficient representation is critical because intermediate workspaces may contain many points, e.g., intermediate workspaces generated by modules composed of binary Stewart platforms can easily have millions of points.

We use the point density array defined in Subsection 2.1 to store all intermediate workspaces. To restore or generate a workspace from a given density array some additional information, e.g. size and volume of each block, is needed. For this purpose, we define the following: The *density set* associated with an intermediate or partial manipulator is a computational structure containing the following information:

- A reference point $\mathbf{x_0} \in I\!R^n$ which defines a point of the workspace in real coordinates. Here $\mathbf{x_0}$ is chosen to represent the middle point of a workspace. That is, each component of $\mathbf{x_0}$ is the middle of the interval bounded by minimal and maximal coordinate values of the workspace.
- The resolution of the discretization, i.e. block dimensions given by $\mathbf{\Delta x} = [\Delta x, \Delta y, \Delta z]^T$,
- The dimensions/length of the array in each direction, either in real (workspace) coordinates, $\mathbf{x_L} = [x_L, y_L, z_L]^T$, or as integers, i_L, j_L, k_L, giving the numbers of pixels for the particular resolution,
- The *density array*, $D(i,j,k)$, of the workspace, which is a N-dimensional array of integers representing the point density of the workspace multiplied by block volume.

We denote a *density set* as

$$\mathcal{D} = \{D, \mathbf{x_0}, \mathbf{\Delta x}, \mathbf{x_L}\}.$$

Note that the orientation of the end effector is not stored since we only discretize in the workspace translational coordinates.

We denote the density set of the i^{th} intermediate workspace as $\mathcal{D}_i^I$, and the density set of the i^{th} partial workspace as $\mathcal{D}_i^P$. In the special case when the manipulator is composed of identical modules, $\mathcal{D}_i^I = \mathcal{D}_i^P$, but generally this will not be the case.

3 The Workspace Mapping Algorithm

The generation of manipulator workspaces and work envelopes is primarily a matter of generating the partial and intermediate workspaces and convolving them in the appropriate way. In this section, the workspace mapping algorithm, which is an efficient way of generating these intermediate and partial workspaces, is presented. Subsection 3.1 presents an overview of the workspace mapping algorithm. Subsection 3.2 describes the implementation

of one iteration of the algorithm in detail. Further details of the implementation, an analysis of the computational complexity of the algorithm in terms of time and memory and the error resulting from the discretization can be found in [6].

3.1 An Overview of the Algorithm

The workspace mapping algorithm determines intermediate workspaces starting at the end-effector and ending at the base. At each step we climb down one module, maintaining an approximation of the intermediate workspace corresponding to the segment of all modules above the current one. In this subsection we explain how the intermediate workspace at a given level has to be transformed to yield the next intermediate workspace including one more module.

Throughout this section B denotes the number of modules of the manipulator under consideration. Index s denotes the sth iteration of the mapping algorithm, $(s = 1, 2, \ldots, B)$, index m denotes the mth module considered in the sth step. The algorithm starts with the last module and propagates backwards. Hence the module number m considered at step s of the algorithm is $m(s) = B - s + 1, \quad s = 1, 2, \ldots, B$, i.e. m is decreasing, while s is increasing.

By our definition W_m^I denotes the intermediate workspace from the top of module m and W_{m-1}^I is the intermediate workspace from the bottom of module m. These two workspaces are related to each other through the set C_m of all possible configurations of module m: $C_m = \{(\mathbf{R}_1^{(m)}, \mathbf{b}_1^{(m)}), (\mathbf{R}_2^{(m)}, \mathbf{b}_2^{(m)}), \ldots, (\mathbf{R}_{2^{J_m}}^{(m)}, \mathbf{b}_{2^{J_m}}^{(m)})\}$ One iteration of workspace mapping determines the density set $\mathcal{D}_{m-1}^I$ (representing the point density of workspace W_{m-1}^I) from given point density $\mathcal{D}_m^I$ and configuration set C_m.

A schematic of this procedure is shown in Figure 3. To simplify the graphical representation a manipulator with only four states per module is considered. Figure 3(a) shows at the left the four configurations (C_m) of the module under consideration in iteration s in terms of the translation and rotation of a frame. The second input to the procedure is the density set $\mathcal{D}_m^I$. It is represented by one rectangle that is divided into blocks of equal size with an integer associated to each of them. An additional reference point represents the position of the center of the rectangle with respect to the origin. The way the density sets (rectangles) are superposed depends on the configurations of the module, as shown on the right of Figure 3(a). An introduction of a wider grid on top of the superposed density sets is shown in Figure 3(b). It only remains to add all entries in each pixel of the new grid to get the output of this iteration: density set $\mathcal{D}_{m-1}^I$.

As can be seen in the picture one iteration only consists of a set of homogenous transformations and the superposition of the results. On a more abstract level this can be seen as a discrete convolution determined by the configurations C_m applied to the input $\mathcal{D}_m^I$.

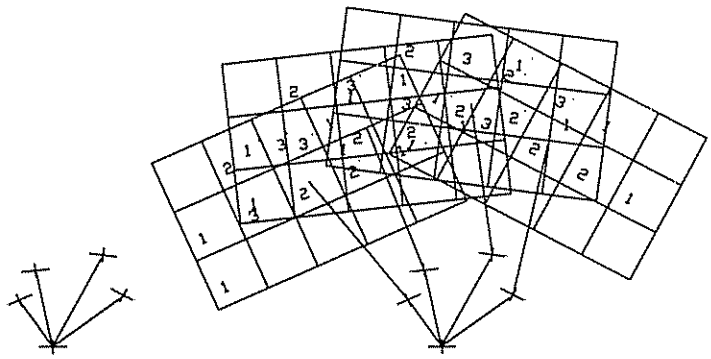

(a) Configurations of one module and resulting overlay of density sets

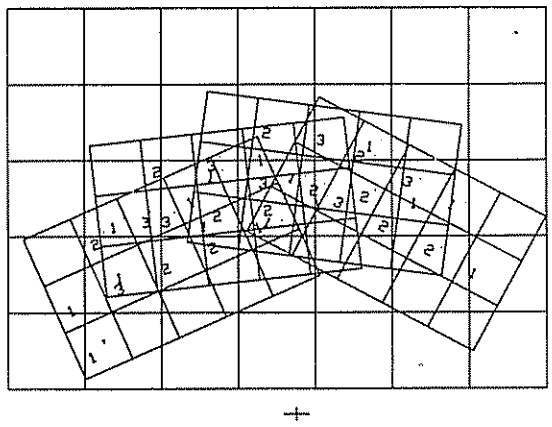

(b) Summing the points in the new grid leads to the next density set

Figure 3: Schematic of one recursion of the workspace mapping algorithm

3.2 Implementation

We start the discussion of the details with a summary of the algorithm: The algorithm starts with the density set $\mathcal{D}_B^I$. The first iteration determines $\mathcal{D}_{B-1}^I$, the second determines $\mathcal{D}_{B-2}^I$, etc. After B iterations the algorithm terminates providing the point density $\mathcal{D}_0^I$ of the complete manipulator arm.

The first implementation detail is the question of the intermediate workspace to start with: Workspace W_B^I is the first workspace to be considered. It describes the location of the end-effector relative to the top of the most distal module. In general this is simply one point, typically the location of the center of the end-effector. However, for the purpose of work envelope generation we

1. Estimate size and location of intermediate workspace W^I_{m-1}. Based on this information:
   (a) Choose the dimensions of a block in the new density array: $\left(\Delta x^{(m-1)}, \Delta y^{(m-1)}, \Delta z^{(m-1)}\right)$
   (b) Based on these dimensions determine the number of fields of the density array in each direction: $\left(i_L^{(m-1)}, j_L^{(m-1)}, k_L^{(m-1)}\right)$
   (c) Allocate sufficient memory for this density array and initialize it with zeros.
   (d) Determine the coordinates of the middle point of the new workspace: $\left(x_0^{(m-1)}, y_0^{(m-1)}, z_0^{(m-1)}\right)$
   (e) Determine the array indices, $\left(i_0^{(m-1)}, j_0^{(m-1)}, k_0^{(m-1)}\right)$, of the middle point of the new array.

2. For all configurations $(\mathbf{R}_l^{(m)}, \mathbf{b}_l^{(m)}) \in C_m$, $(l = 1, \ldots, 2^{J_m},)$ apply the corresponding homogeneous transformation to the density array D^I_m:

   For all indices (i, j, k) for which the entry $D^I_m(i, j, k)$ of the density array D^I_m is not zero:

   (a) Calculate the vector $\mathbf{x} = (x(i), y(j), z(k))^T$ from the array indices (i, j, k).
   (b) Calculate the coordinate vector $\mathbf{x}' = \mathbf{R}_l^{(m)}\mathbf{x} + \mathbf{b}_l^{(m)} \in W^I_{m-1}$.
   (c) Find the array indices $\left(i', j', k'\right)$ of $\mathbf{x}'$ in the new array.
   (d) Increment the entry of the block of the new array by the corresponding entry of the old array:

$$D^I_{m-1}(i', j', k') \quad \leftarrow \quad \left(D^I_{m-1}(i', j', k') + D^I_m(i, j, k)\right)$$

Figure 4: Implementation of one recursion of the workspace mapping algorithm

choose W^I_B to be the discretized shape of the end-effector including the upper part of the last module. In any case density set $\mathcal{D}^I_B$ can easily be determined from this information.

A schematic of one iteration is given in Figure 3 and was explained in the previous subsection. Figure 4 lists the major steps of the implementation of one iteration and is further explained below.

The first block in Figure 4 describes the administrational part of an iteration: an estimate of size and location of the intermediate workspace to be calcaluted is needed, the resolution has to be chosen and memory has to be allocated accordingly. For details we again refer the reader to [6].

To estimate size and location of workspace W^I_{m-1}, all 2^{J_m} homogeneous transforms are applied to the eight corners of the density array D^I_m (four for the planar case). The resulting maximal and minimal values in each coordinate axis provide a conservative estimate for the boundaries of the next density array, D^I_{m-1}. An additional reduction procedure is implemented to reduce a resulting memory overhead after the workspace is calculated. The computational complexity for the estimate and the reduction procedure are not significant compared to the essential mapping process described in the second block.

The second block in Figure 4 describes the implementation of the homogenous transformations. They are implemented by steps (a) - (d), in the interior of the lower block, which are performed for each configuration and for all indices corresponding to non-zero entries in D^I_m. Hence it is the main contribution to the computational complexity of the algorithm. It is therefore worthwhile to discuss these steps in more detail:

We consider only one iteration. To eliminate indices that complicate the presentation the following notation is used. All variables belonging to workspace W^I_m or density set $\mathcal{D}^I_m$ have names without superscript, while variables belonging to W^I_{m-1} or $\mathcal{D}^I_{m-1}$ have a superscript $'$. Furthermore we restrict the description to one particular configuration $(\mathbf{R}, \mathbf{b}) = (\mathbf{R}_l^{(m)}, \mathbf{b}_l^{(m)}) \in C_m$.

Now we consider one particular block of the input density set $\mathcal{D}^I_m$ specified by the indices (i, j, k). The corresponding entry of the density array is denoted $d = D^I_m(i, j, k)$. The operations to be performed are:
(a) The middle point of block with index (i, j, k) is taken as the refernce for the block. Its coordinates in the workspace are:

$$\mathbf{x} = \begin{pmatrix} \Delta x & 0 & 0 \\ 0 & \Delta y & 0 \\ 0 & 0 & \Delta z \end{pmatrix} \begin{pmatrix} i \\ j \\ k \end{pmatrix} + \begin{pmatrix} x_0 - i_0\Delta x \\ y_0 - j_0\Delta y \\ z_0 - k_0\Delta z \end{pmatrix}$$

(b) The homogenous transformation corresponding to configuration $(\mathbf{R}, \mathbf{b})$ is applied to this reference point:

$$\mathbf{x}' = \begin{pmatrix} x' \\ y' \\ z' \end{pmatrix} = \mathbf{R}\mathbf{x} + \mathbf{b}$$

(c) The indices (i', j', k') of $\mathbf{x}'$ for the output density set $\mathcal{D}^I_{m-1}$ are:

$$\begin{pmatrix} i'(x') \\ j'(y') \\ k'(z') \end{pmatrix} = \begin{pmatrix} \text{round}\left(i'_0 + (x' - x'_0)/\Delta x'\right) \\ \text{round}\left(j'_0 + (y' - y'_0)/\Delta y'\right) \\ \text{round}\left(k'_0 + (z' - z'_0)/\Delta z'\right) \end{pmatrix}$$

(d) Finally the entry of block (i', j', k') in density set $\mathcal{D}^I_{m-1}$ is incremented by $d = D^I_m(i, j, k)$.

Note, that the entries of the same density array D^I_{m-1} are changed while handling all $l = 1, \ldots, 2^{J_m}$ configurations, without reinitializing. This implements the superposition (or convolution) of all parts of workspace W^I_{m-1}.

Steps (a)-(c) are affine transformations, the last one followed by a rounding procedure. This can be represented as one composite affine transformation followed by rounding which considerably improves the performance of the operation. The described procedure is performed in constant time for each block. Choosing a fixed number of pixels for all intermediate workspaces, has shown good performance. As a result the error grows quadratically in the number of modules B with a very small factor. The amount of required memory is linear in the number of modules as is the time requirement, see [6].

4 Applications and Examples

In this section we present examples of workspaces generated using the workspace mapping algorithm, and show how the algorithm has to be altered to generate work envelopes. In these examples the algorithm is applied to a binary truss manipulator. Each module has the same structure as the modules of the manipulator described in Section 1 and illustrated in Figure 1 and 2. Only the number of modules varies.

Figure 5 (a)-(c) show the results for a binary truss manipulator with 5,8 and 14 platforms respectively, each with actuator strokes stated earlier. Figure 5 (a), which presents the workspace of the manipulator with 5 platforms, can be compared to the exact results shown in Figure 2. Note, that the length scales of the figures differ for different numbers of platforms.

In order to generate the work envelope, we modify the algorithm by choosing a different start workspace than before. Previously a single point was used representing the center of the end-effector. Now we choose a contour that represents the shape of the end-effector. Here we simply use a line representing the upper base of the most distal module. Application of the algorithm sweeps this line (contour) through the plane in discrete steps corresponding to all possible configurations. The algorithm can also be modified to allow smaller steps of the sweeping procedure than given by the discrete configurations. This way a continuous sweeping contour is generated. A

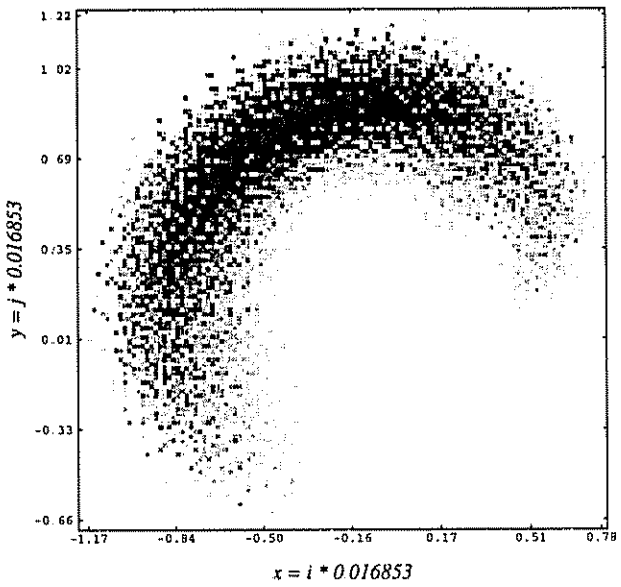

Figure 5(a): Density of a manipulator with 5 modules (15 Bits), $r_5 = 0.018858$

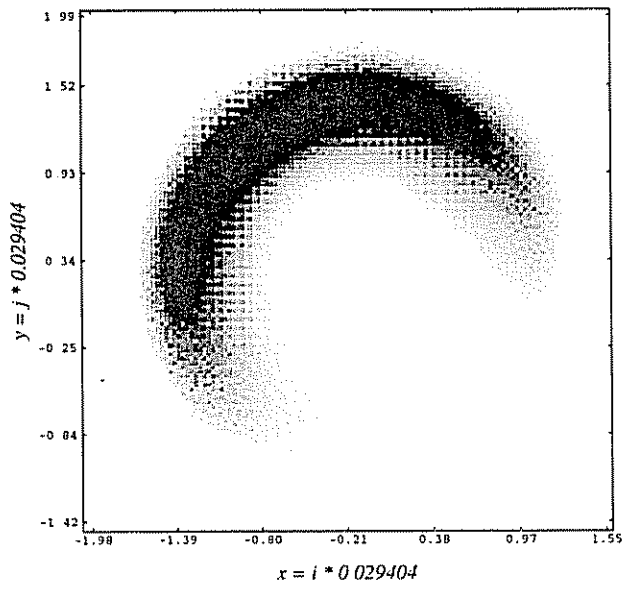

Figure 5(b): Density of a manipulator with 8 modules (24 Bits), $r_8 = 0.041790$

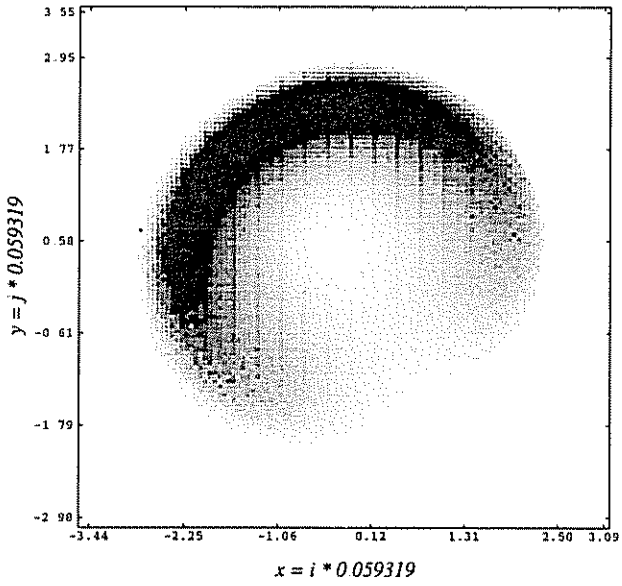

Figure 5(c): Density of a manipulator with 14 modules (42 Bits), $r_{14} = 0.146833$

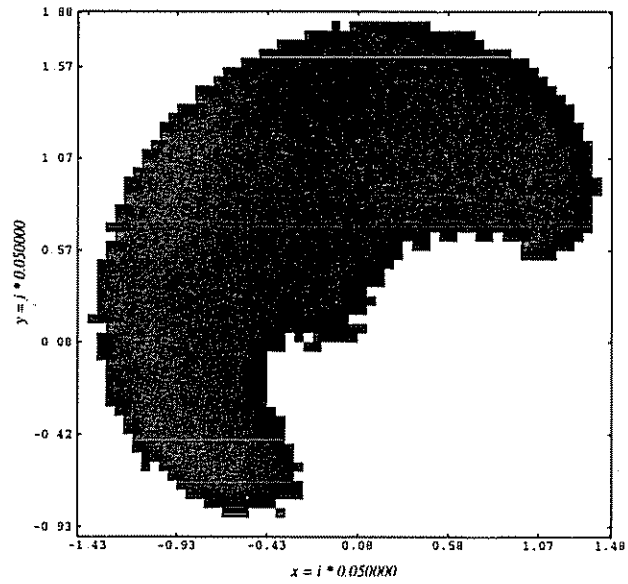

Figure 6: Work envelope of a manipulator with 9 modules (27 Bits)

further simplification is that the number of points for each pixel is not stored, but instead whether or not it is empty (0 or 1).

To calculate the work envelope of a manipulator consisting of m modules, this modified version of the mapping algorithm is applied to the partial manipulators composed of m, $m-1$, ..., 1 modules and the resulting partial workspace are superposed. The result will be a fairly reliable representation of the work envelope. Furthermore, if the modules are all the same, the algorithm has to be applied only once, since $D_m^I = D_m^P$.

Figure 6 shows the work envelope for the case when the joint stops are closer together than in the previous examples, (3/20,4/20), and the width of each platform is chosen as before (4/20).

5 Conclusions

This paper has presented an efficient algorithm for generating approximate workspaces and work envelopes of robotic manipulators with binary (two-state) actuators. Examples were provided for the case of a planar binary variable geometry truss with up to 20 modules. While the focus of this paper was binary manipulators, the method is applicable to general manipulators if their joint range is discretized and represented using an appropriate number of bits.

References

[1] G.S. Chirikjian. A binary paradigm for robotic manipulators. In *Proceedings of the 1994 IEEE International Conference on Robotics and Automation*, San Diego, CA, May 1994.

[2] J. Rastegar and P. Deravi. The effect of joint motion constraints of the workspace and number of configurations of manipulators. *Mech. Mach. Theory*, 22(5):401 - 409, 1987.

[3] R. G. Selfridge. The reachable workarea of a manipulator. *Mech. Mach. Theory*, 18(2):131 - 137, 1983.

[4] Alok Kumar and Kenneth J. Waldron. Numerical plotting of surfaces of positioning accuracy of manipulators. *Mech. Mach. Theory*, 16(4):361 - 368, 1980.

[5] Dibakar Sen and T. S. Mruthyunjaya. A discrete state perspective of manipulator workspaces. *Mech. Mach. Theory*, 29(4):591 - 605, 1994

[6] I. Ebert-Uphoff and G.S. Chirikjian. Efficient workspace generation for binary manipulators with many actuators. Journal of Robotic Systems, June 1995 (in press).